Single-crystalline $Mg_xZn_{1-x}O$ ($0 \leq x \leq 0.25$) nanowires on glass substrates obtained by a hydrothermal method: growth, structure and electrical characteristics

2005 Nanotechnology 16 1105

(http://iopscience.iop.org/0957-4484/16/8/019)

INSTITUTE OF PHYSICS PUBLISHING NANOTECHNOLOGY
Nanotechnology **16** (2005) 1105–1111 doi:10.1088/0957-4484/16/8/019

Single-crystalline $Mg_xZn_{1-x}O$ ($0 \leqslant x \leqslant 0.25$) nanowires on glass substrates obtained by a hydrothermal method: growth, structure and electrical characteristics

Chia Ying Lee[1], Tseung Yuen Tseng[1,3], Seu Yi Li[2] and Pang Lin[2]

[1] Department of Electronic Engineering and Institute of Electronics, National Chiao Tung University, Hsinchu 300, Taiwan, Republic of China
[2] Institute of Materials Science and Engineering, National Chiao Tung University, Hsinchu 300, Taiwan, Republic of China

E-mail: tseng@cc.nctu.edu.tw

Received 27 December 2004, in final form 22 March 2005
Published 17 May 2005
Online at stacks.iop.org/Nano/16/1105

Abstract
Single-crystalline $Mg_xZn_{1-x}O$ ($0 \leqslant x \leqslant 0.25$) nanowires (MZO NWs) were synthesized on glass substrates by a hydrothermal method using a mixture of an aqueous solution of zinc nitrate hexahydrate, magnesium nitrate hexahydrate and diethylenetriamine at temperatures that ranged from 75 to 105 °C. X-ray diffraction, scanning electron microscopy and transmission electron microscopy investigations were carried out to characterize the crystallinity, surface morphologies and orientations of these nanowires, respectively. These nanowires with direct band gaps ranging from 3.21 to 3.95 eV emitted ultraviolet photoluminescence from 406 to 397 nm at room temperature as the Mg content increased. Field emission measurements revealed that the turn-on electric field and threshold electric field (current density of 1 mA cm^{-2}) of ZnO NWs are 1.6 and 2.1 V μm^{-1} with the β value of 3340. Therefore, low temperature synthesized MZO NWs ($0 \leqslant x \leqslant 0.25$) with modulated band gaps may be applied in solar cells, light emission devices and other nanoheterojunction devices in the future.

1. Introduction

With the evolution of nanotechnology, one-dimensional (1D) nanostructures, including nanowires (NWs), nanotubes and nanobelts, play an important role in the potential application of photonic, electro-optical and electronic devices for their unique physical and chemical properties [1–3]. These NWs have been synthesized by various processes, such as vapour–liquid–solid (VLS) growth [4], metal–organic vapour phase epitaxy (MOVPE) procedures [5], molecular beam epitaxy (MBE) [6], pulsed laser deposition (PLD) [7], template methods [8] and hydrothermal methods [9]. In particular, the hydrothermal method is regarded as preferable to other growth methods since there are many advantages to adopting this NWs growth method: the possibility of dopant incorporation, catalyst-free growth, low cost, low reaction temperature, large scale production and environment friendliness.

ZnO, a wide band gap (3.4 eV) and large exciton binding energy (60 meV) material, has drawn much attention for applications in ultraviolet (UV) laser devices [10], phosphors [11], transparent conducting films for solar cells [12] and flat panel displays [13]. Recently, it has been reported that band gap tunable $Mg_xZn_{1-x}O$ (MZO) films are formed by mixing MgO ($\Delta E_g = 7.8$ eV) with ZnO, and the direct band gap varies from 3.3 to 4.0 eV as the Mg content increases [14]. The crystal structure of MZO is quite

[3] Author to whom any correspondence should be addressed.

Table 1. Relationship among composition of synthesized MZO NWs, concentration of Mg in the solution and pH of the solution.

x value in MZO based on EDX results	Concentration of Mg in the solution (M)	pH of the solution
$x = 0.00$	0.00	7.0
$x = 0.05$	0.02	7.0
$x = 0.10$	0.06	7.2
$x = 0.15$	0.10	7.2
$x = 0.20$	0.15	7.4
$x = 0.25$	0.25	7.4

similar to the ZnO one, as the ionic radii of Mg^{2+} (0.57 Å) and Zn^{2+} (0.60 Å) [15] are comparable. With a similarity in crystal structure and modulation in the band gap, MZO/ZnO is expected to be a potential quantum well heterostructure for optoelectronic device use.

Although MZO NWs and MZO/ZnO NW heterostructures have already been synthesized by MOCVD [5] and MBE [6], these processes are expensive, toxic and power consuming. In order to overcome all these problems, the hydrothermal method is employed in this study to provide a low temperature process for fabricating MZO NWs on a glass substrates. The microstructures, surface morphologies, optical properties and field emission characteristics of the MZO NWs were investigated.

2. Experimental procedure

To prepare the NWs by a hydrothermal method on an ITO glass substrate (Ritec Co., 40 Ω/□), 70 Å ultrathin ZnO film was deposited on the substrate by rf sputtering (13.56 MHz) under Ar sputtering gas at 20 mTorr. Then, the coated glass substrates were put into an aqueous solution (Milli Q, 18.2 MΩ cm) of zinc nitrate hexahydrate ($Zn(NO_3)_2{\cdot}6H_2O$, 0.01 M), magnesium nitrate hexahydrate ($Mg(NO_3)_2{\cdot}6H_2O$) and diethylenetriamine (HMTA, $C_6H_{12}N_4$, 0.01 M) in a sealed vessel at temperatures from 75 to 105 °C for various reaction times from 10 min to 2 h. The surface morphologies of these samples were observed by atomic force microscopy (AFM, DI NS3a) in order to realize the crystal growth in the course of the process. The microstructure and properties of the 2 h synthesized NWs that had been cleaned with deionized (DI) water and dried in a vacuum oven at room temperature for 5 h were investigated. The chemical composition of the MZO NWs formed was controlled by changing the pH and the Mg concentration in the aqueous solution (table 1). The chemical composition and microstructures were confirmed by field emission scanning electron microscopy (FE-SEM, Hitachi S-4700I, Japan) coupled with an energy dispersive x-ray analyser (EDX, Oxford, England) and high resolution transmission electron microscopy (HR-TEM, Philips tecani-20), respectively. The crystal structures of the MZO NWs were examined by means of x-ray diffraction (XRD, MAC Science, MXP18, Japan). Room temperature optical properties were confirmed by a UV–visible spectrometer (UV-VIS, Hitachi 557, Japan) and photoluminescence analyser (PL, Hitachi F-4500, Japan) with a Xe lamp as an excitation source (325 nm). A Keithley 237 source–measure unit was used for measuring

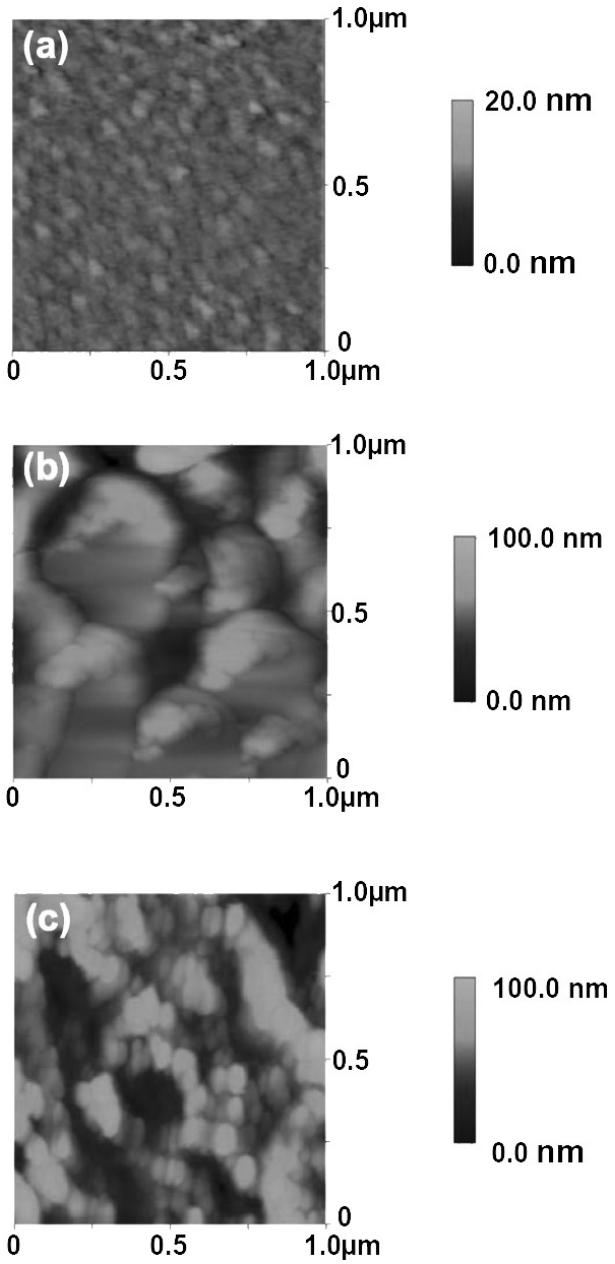

Figure 1. AFM micrographs of (a) the as-deposited ZnO seeding layer surface, (b) a 10 min hydrothermal grown ZnO surface, (c) a 10 min hydrothermal grown MZO ($x = 0.10$) surface.

the current–voltage (I–V) and field emission characteristics. The field emission characterizations were carried out in a vacuum chamber at a base pressure of 1×10^{-6} Torr at room temperature. A copper electrode probe adopted as an anode with the area of 7.1×10^{-3} cm^2 was placed at a distance of 450 μm from the tips of the NWs and was adjusted by a precision screwmeter with an accuracy of ± 0.1 μm.

3. Results and discussion

The AFM photographs shown in figure 1 reveal the initial nucleation of hydrothermal growth. Figure 1(a) depicts an AFM image of the 70 Å thick rf-sputtered ZnO film,

indicating that the grain size and surface roughness of this film are about 50 and 0.837 nm, respectively. This rf-sputtered ZnO film served as a seeding layer for the following ZnO NWs grown hydrothermally on the substrate. Then, these coated substrates were put in aqueous solutions A of $Zn(NO_3)_2{\cdot}6H_2O$ and HMTA and B of $Zn(NO_3)_2{\cdot}6H_2O$, HMTA and $Mg(NO_3)_2{\cdot}6H_2O$ (0.02 M) at 85 °C for 10 min in the sealed vessels, to observe the influence of Mg on the initial nucleation. The surface morphology of the sample put in solution A, shown as figure 1(b), indicates surface grain size of 250 nm and surface roughness of 11.52 nm, while the surface morphologies of the sample put in solution B (figure 1(c)) are those of round surface grains with a grain size of 80 nm and surface roughness of 75.93 nm. Such different morphologies, which arise from different nucleation–growth mechanism, may be explained by the difference in surface energy between ZnO and MZO that leads to the formation of ZnO film on the surface of coated substrate in solution A and islands of MZO being formed on the substrate surface in solution B.

The cross-section FE-SEM image of ZnO NWs immediately grown on the ITO glass substrate before cleaning shown in figure 2(a) depicts that some impurities, probably including $Zn(NO_3)_2$, HMTA and ZnO crystal, appear on the top of NWs. Therefore, we cleaned such 2 h synthesized NWs with DI water to remove those impurities and dried them in the vacuum oven for 5 h. After cleaning, there are no impurities on top of the NWs as shown in figure 2(b). Thus, we employed the above cleaning process for all of the NWs grown. The FE-SEM images of MZO NWs ($0 \leqslant x \leqslant 0.25$) on glass substrates are shown in figures 2(b)–(g), indicating that the surface morphologies of these MZO NWs depend on the amount of Mg. The chemical composition of these NWs was confirmed by the EDX unit attached to the FE-SEM (not shown here). This analysis was focused on the individual NWs to avoid the influence of underlying ZnO layer. As shown in figure 2(b), a 200 nm thick ZnO film deposited on the glass substrate during hydrothermal growth and well-aligned ZnO NWs grown on such a ZnO film have acicular tips with diameter of 50 nm and length of 0.5 μm. This ZnO film is thicker than the rf-sputtered seeding layer. Such a thick ZnO film which gradually regulates the orientation on the substrate is suitable for the well-aligned growth of ZnO NWs. The NWs have lower number density since some precursors were consumed during the ZnO film deposition. In contrast, the MZO ($0.05 \leqslant x \leqslant 0.20$) NWs grown on thinner films have blunt tips, slender roots, larger number density and random distribution (figures 2(c)–(e)). The films hydrothermally grown on the coated substrates are thinner, and are composed of columnar grains. This polycrystalline film with the distinct orientation results in the non-vertical random distribution growth of MZO NWs. The MZO NWs grow larger in size on the addition of Mg in the aqueous solution. The average diameter of these MZO NWs is from 80 to 100 nm and the length is from 0.5 to 1 μm. The larger MZO NWs may be attributed to the larger part of the precursor being consumed during the MZO NWs growth as compared with the ZnO film growth. The surface energy difference between ZnO and MZO also affects the geometry of these NWs, which is demonstrated in figure 1. The ZnO NWs have a uniform diameter in stems, while the MZO NWs have larger diameter

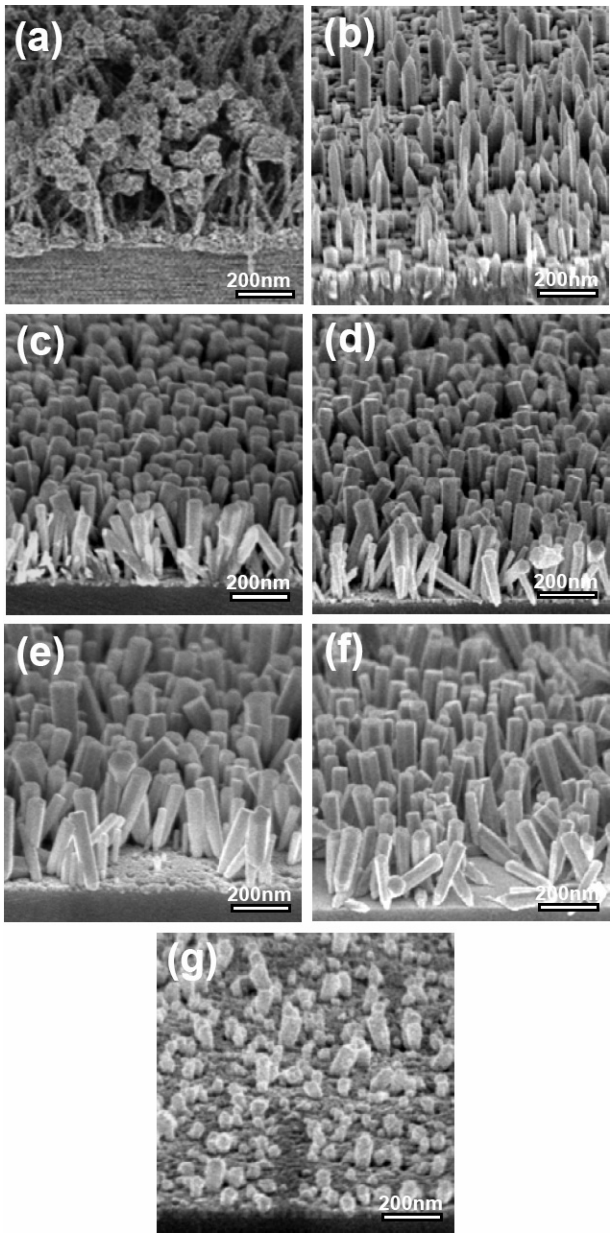

Figure 2. (a) Cross-section FE-SEM micrographs of as-grown ZnO NWs, and the morphologies of MZO NWs with various values of x: (b) $x = 0$, (c) $x = 0.05$, (d) $x = 0.10$, (e) $x = 0.15$, (f) $x = 0.20$ and (g) $x = 0.25$.

in stems and narrow roots on the substrate. The MZO NWs were grown on the MZO islands formed on the seeding layer in the initial stage of the hydrothermal process which leads to the formation of narrow roots of MZO NWs on the substrate after reaction. In this solid solution process, the Mg atoms substitute for the Zn sites. As the Mg content is increased to 0.25, the growth of MZO NWs slows down. The diameter of these MZO NWs ranges between 80 and 100 nm, and the length of these is reduced to 150 nm. Due to the difference in radii of Mg^{2+} and Zn^{2+} ions, the solubility of Mg in the ZnO NWs decides the upper limitation of the hydrothermal growth.

Figure 3(a) shows the XRD patterns of MZO NWs with various Mg contents. Single-phase MZO NWs could be

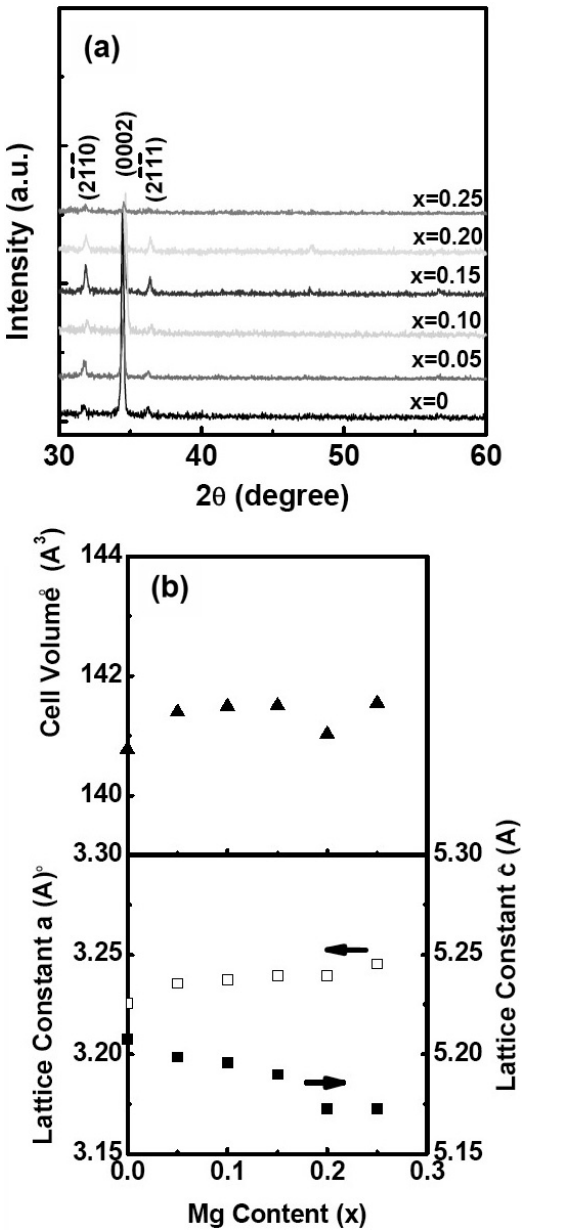

Figure 3. (a) XRD spectra of MZO NWs with various x values indicated. (b) a- and c-axis lattice parameters and cell volume of MZO NWs.

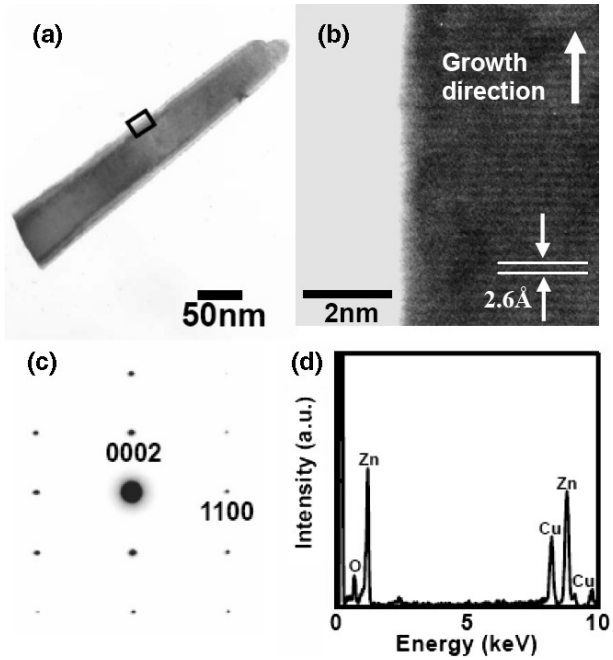

Figure 4. (a) TEM micrograph of ZnO NWs. (b) HR-TEM image of ZnO NWs in the rectangular box region in (a). (c) SAED pattern of ZnO NWs marked in the boxed region of (a). (d) EDX spectra of ZnO NW in the marked region of (a).

synthesized with x up to 0.25 by a hydrothermal method. With the increase in Mg content of the MZO NWs, it is observed that the crystal structures of these NWs are wurtzite type and no other impurities appear. As shown in the figure, the peak intensity of MZO NWs ($x = 0.25$) is smaller than others, for there are fewer NWs grown on the substrate. The lattice constant and corresponding cell volume measured from the XRD patterns are shown as a function of the Mg content in figure 3(b). With the increase of the Mg content from 0 to 0.25, the c-axis lengths calculated from the (0002) peak of the NWs decrease from 5.21 to 5.17 Å, while the a-axis lengths calculated from the $(2\bar{1}\bar{1}0)$ one increase from 3.23 to 3.25 Å. However, the cell volumes of these NWs are almost unchanged. The addition of MgO to ZnO forms a solid solution with the wurtzite structure, and the deviation of the lattice constants may be due to the small difference of ionic radii of Mg^{2+} and Zn^{2+}.

HR-TEM images and the corresponding selected area electron diffraction (SAED) pattern are shown in figure 4, which illustrates the appearance and crystal structure of the NWs. The ZnO NW (figures 4(a) and (b)) with an acicular tip, uniform diameter of 50 nm and length of 0.4 μm is found growing in the [0002] direction. The distance between parallel [0002] lattice fringes of the ZnO NW is 2.60 Å, and the lattice constants calculated from the SAED pattern (figure 4(c)) are $a = b = 3.23$ Å and $c = 5.21$ Å, which are consistent with the XRD result. The chemical compositions of ZnO NW in the rectangular box region of figure 4(a) were determined by the EDX spectrometer attached to the HR-TEM. Figure 4(d) is the EDX spectrum of ZnO NW and it reveals that zinc (52%) and oxygen (48%) are the constituent parts of ZnO NWs.

Upon studying the shape of the ZnO NW, it is found that the NW is straight with a smooth surface and uniform composition. But the morphology of the MZO NW ($x = 0.10$; figure 5(a)) is quite different from that of the ZnO NW. In figure 5(a), the MZO NW has a blunt tip and a slender root with the diameter of 80 nm and length of 0.5 μm. It is obvious that those MZO NWs grow along the [0002] direction, and the distance between two [0002] lattice fringes of MZO NW is 2.59 Å. The SAED pattern (figure 5(c)) can be indexed to the reflections of hexagonal MZO structure, and the lattice constants of MZO are $a = b = 3.24$ Å and $c = 5.20$ Å. The chemical compositions of this MZO NW ($x = 0.1$) in the rectangular box regions of figure 5(a) were analysed by means of the EDX spectrum (figure 5(d)), which shows that its chemical composition is zinc (41%), magnesium (11%) and

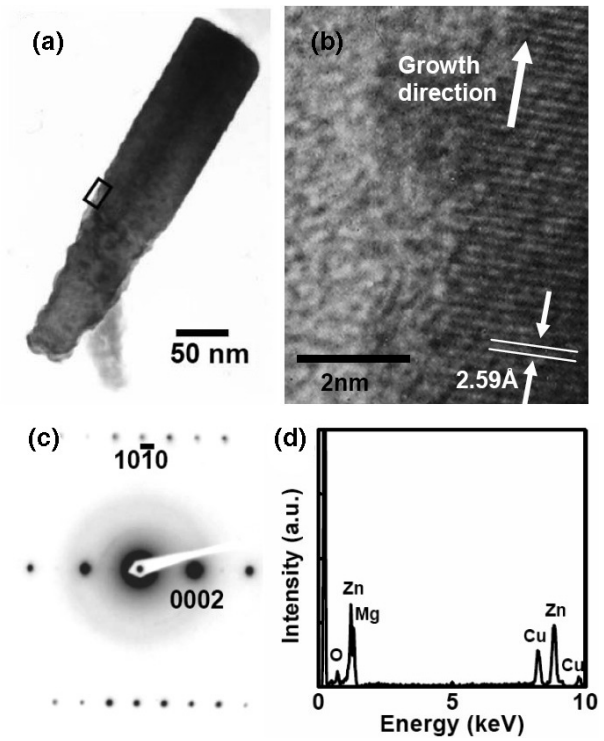

Figure 5. (a) TEM micrographs of MZO ($x = 0.1$) NWs. (b) HR-TEM image of MZO NWs in the rectangular box region of (a). (c) SAED pattern of the MZO NWs of the marked box region of (a). (d) EDX spectra of the MZO NW in the boxed region of (a).

oxygen (48%). Hence, the MZO NW could be synthesized by a hydrothermal method with a blunt tip, slender root and uniform chemical composition.

Room temperature transmission spectra of the MZO NWs ($0 \leqslant x \leqslant 0.25$) fabricated on the glass substrates were recorded by a UV–visible spectrometer (figure 6(a)). As shown in the figure, the transmittances of MZO NWs ($0 \leqslant x \leqslant 0.2$) are 50–60% in the range from 380 to 600 nm and the UV light is absorbed by these NWs. These transmittances are lower than those of the MZO films reported by other groups [14]. It is believed that the rough surface of MZO NWs scatters part of the light, causing the transmittance of these samples to decrease. The transmittance of MZO NWs ($x = 0.25$) is increased to 75% for the shorter nanowires and smaller number density of NWs. One sharp absorption edge appears for the ZnO NWs, while two absorption steps could be observed for the MZO NWs. While the first absorption edge of MZO NWs shifts from 375 to 305 nm, the second absorption edge results from the ZnO buffer layer on the glass substrates in the range from 360 to 365 nm. To realize the relationship between the transmission spectra and the band gap, the absorption coefficient α is estimated after considering the reflection loss of the glass substrate, and α^2 is plotted as a function of photon energy ($h\nu$) as shown in figure 6(b). The absorption edge is used to determine the energy band gap (E_g) of MZO NWs. The band gap of MZO NWs as a function of Mg content is shown in figure 6(c). The band gap of ZnO NWs synthesized by the hydrothermal method is 3.21 eV, which then increases to 3.95 eV for the MZO ($x = 0.25$) NWs. With the increase of the Mg content in the MZO NWs, the band gaps of the

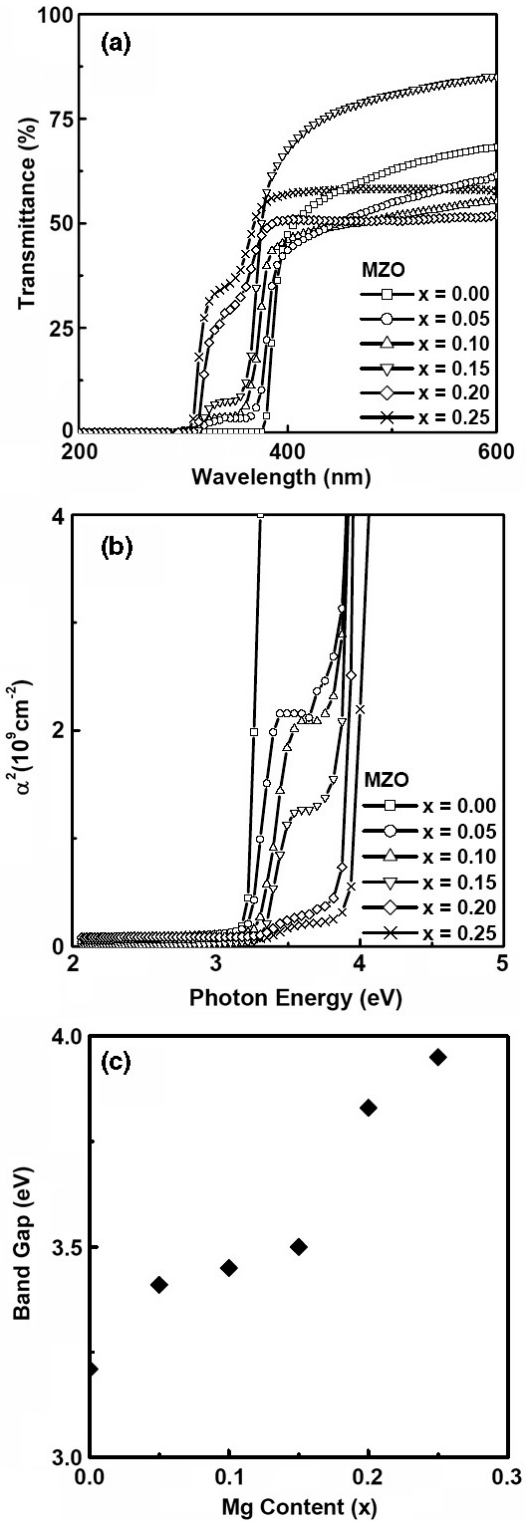

Figure 6. (a) UV–visible transmission spectra of MZO ($0 \leqslant x \leqslant 0.25$) NWs. (b) A plot of α^2 versus photon energy for MZO ($0 \leqslant x \leqslant 0.25$) NWs. (c) Energy band gap as a function of Mg composition.

MZO NWs increase because of the broadening effect [15] which takes place as the carriers feel different potentials for the local concentration of the substituting elements in the crystal. Therefore, by adding various Mg contents in the MZO NWs,

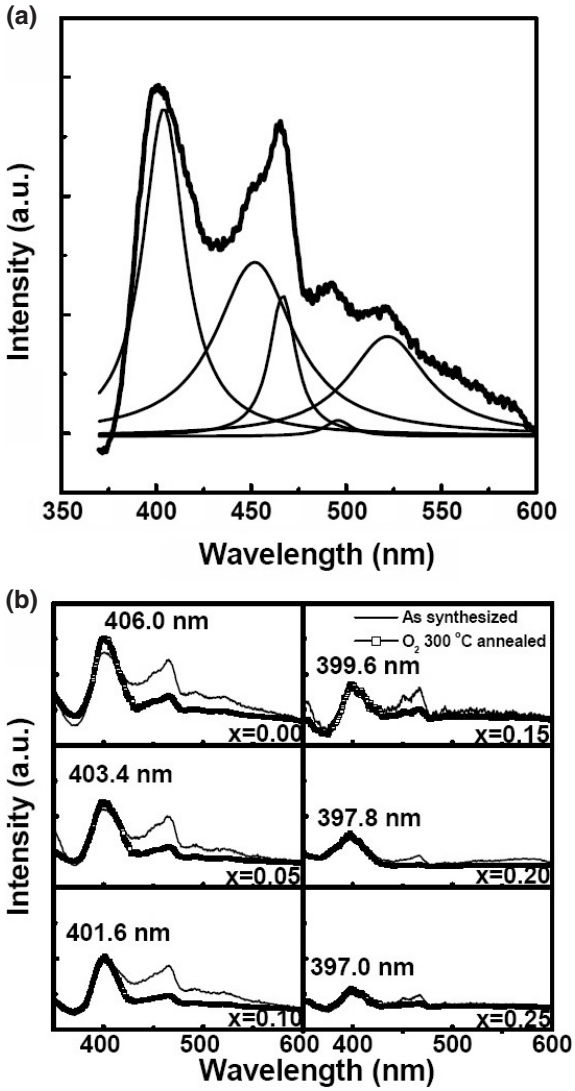

Figure 7. (a) PL spectra of ZnO NWs and deconvolution of the spectra. (b) PL spectra of as-synthesized and 300 °C O_2 annealed MZO ($0 \leqslant x \leqslant 0.25$) NWs.

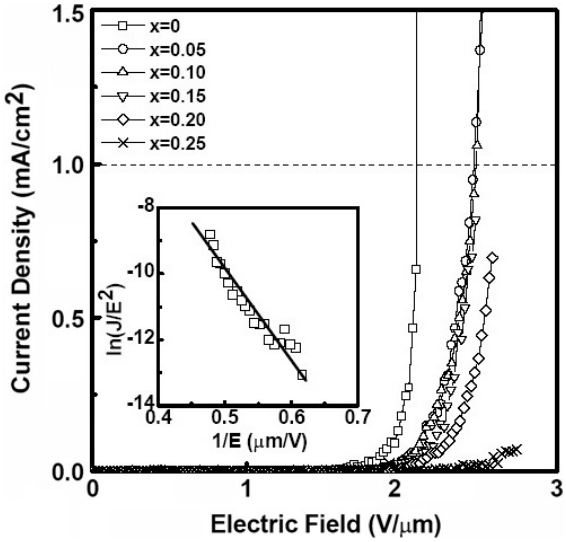

Figure 8. Field emission current–voltage curves of MZO ($0 \leqslant x \leqslant 0.25$) NWs. (The inset is the Fowler–Nordheim plot of ZnO NWs.)

the band gap can be modulated. Similar lattice constants of MZO and ZnO could be exploited for the fabrication of MZO/ZnO nanowire heterojunctions, which may be used in various optoelectronic applications.

Figure 7 shows the photoluminescence spectra of MZO NWs with $x = 0$, 0.05, 0.10, 0.15, 0.20 and 0.25. These NWs were excited by a Xe lamp ($\lambda = 325$ nm) at room temperature. As shown in figure 7(a), ZnO NWs emit a strong emission at 406 nm (3.05 eV) and luminescence at 465 nm (2.66 eV), 495 nm (2.52 eV) and 520 nm (2.38 eV). The UV emission is due to band edge emission of ZnO, and the band edge emission peak shifts from 406 to 397 nm (3.12 eV) as the Mg content increases to 0.25 in the MZO NWs (figure 7(b)). This UV photoluminescence characteristic reveals the Stokes shift of the solid solution [16]. The band edge emission intensity of ZnO NWs is the highest, while that of MZO NWs gets lower as the Mg content increases. It can be demonstrated that the randomly distributed MZO NWs scattered the emission of light which results in the weaker optical intensity. As the Mg content increases to 0.25, the weakest band edge emission intensity appears due to the shorter optical cavities provided by the NWs. Furthermore, there is a blue emission located at 465 nm in the MZO NWs ($0 \leqslant x \leqslant 0.25$). This emission of 465 nm may be associated with the oxygen deficiency in these NWs [8, 17]. The oxygen deficiency is related to the growth condition of these NWs in the aqueous solution. The MZO NWs grow on the seeding layer while HMTA releases OH^- slowly in the solution. The OH^- ions are finite, but metal ions, such as Zn^{2+} and Mg^{2+}, are sufficient in this environment. Therefore, oxygen is lacking in the MZO NWs fabricated by the hydrothermal method. It has been reported that the luminescences at 495 and 520 nm of ZnO are caused by the deep level [18] and singly ionized oxygen vacancies [19]. After annealing at 300 °C in the oxygen atmosphere, the location of band edge emission is unchanged, but the emissions expected to be caused by oxygen deficiency, deep levels and singly ionized oxygen vacancies of these MZO NWs ($0 \leqslant x \leqslant 0.25$) are decreased because these defects are removed upon annealing in the oxygen atmosphere without phase separation.

Field emission characteristics of the MZO NWs ($0 \leqslant x \leqslant 0.25$) are shown in figure 8. As shown in the figure, the ZnO NWs on the ITO substrate perform better as regards field emission properties. The turn-on electric field (E_{on}) and threshold electric field (E_{th}) under the current density of 1.0 mA cm^{-2} for ZnO NWs are 1.6 and 2.1 V μm^{-1}, respectively. As the Mg content increases, the E_{on} and E_{th} of the MZO ($0.05 \leqslant x \leqslant 0.25$) NWs increase. The Fowler–Nordheim (FN) plot for ZnO NWs on ITO glass is depicted in the inset of figure 8, indicating that the measured data fit the following relationship:

$$\ln\left(\frac{J}{E^2}\right) = \left(\frac{-B\phi^{3/2}}{\beta}\right)\left(\frac{1}{E}\right) + \ln\left(\frac{A\beta^2}{\phi}\right) \qquad (1)$$

where J is the current density, E the applied field, ϕ the work function of the emitter, β the field enhancement factor,

$A = 1.56 \times 10^{-10}$ (A eV V^{-2}) and $B = 6.83 \times 10^3$ (V $eV^{-3/2}$ μm^{-1}). β for these samples can be calculated from the slopes of the FN plots by adopting the work function of ZnO (5.37 eV) [20]. The β values of MZO NWs with Mg contents of 0, 0.05, 0.10, 0.15, 0.20 and 0.25 are 3340, 2753, 2688, 2644, 2489 and 2214, respectively. The β value decreases as the Mg content increases. It is suggested that the ZnO NWs on the ITO glass substrate with acicular tips provided a larger field enhancement factor, while the blunt-tip MZO NWs contribute to the smaller field enhancement factor. With the Mg content increasing up to 0.25, the low emission current density is observed for fewer low aspect ratio emitters on the substrate. On the basis of the previous studies reported by our group [13], we know that vapour–liquid–solid (VLS) synthesized ZnO NWs exhibit better field emission properties than the hydrothermal synthesized ones because of the higher aspect ratio and smaller tip diameter. However, the applications of VLS synthesized NWs are restricted, since it is difficult to integrate the VLS process with microelectronic devices because of the non-uniformity and high reaction temperature. As a result, the hydrothermal synthesized ZnO NWs are suitable materials for electric and electro-optical device use.

4. Summary

In summary, single-crystalline $Mg_xZn_{1-x}O$ nanowires ($0 \leqslant x \leqslant 0.25$) on glass substrates are synthesized by a hydrothermal route at 75–105 °C. The crystal structure of MZO NWs is similar to that of ZnO NWs, while the morphology of MZO NWs is slightly different from that of the ZnO NWs. Room temperature transmission spectra illustrated that the band gap of the MZO NWs shifted from 3.21 to 3.95 eV, and the band edge emission from 406 to 397 nm, on adding various amounts of Mg in the ZnO NWs. Furthermore, the ZnO NWs with the acicular tips exhibit better emission properties than MZO NWs. Therefore, the low temperature synthesized MZO NWs with modulated band gaps and similar crystal structure to ZnO MWs may be appropriate for fabricating MZO/ZnO nanoheterojunction optoelectronic and field emission devices.

Acknowledgment

This work was supported by the National Science Council of ROC Contract No NSC 93-2215-E-009-048.

References

[1] Huber T E, Nikolaeva A, Gitsu D, Konopko L, Foss C A Jr and Graf M J 2004 *Appl. Phys. Lett.* **84** 1326
[2] Xia T S, Register L F and Banerjee S K 2004 *J. Appl. Phys.* **95** 1597
[3] Bai X D, Gao P X, Wang Z L and Wang E G 2003 *Appl. Phys. Lett.* **82** 4806
[4] Li S Y, Lee C Y and Tseng T Y 2003 *J. Cryst. Growth* **247** 357
[5] Park W I, Yi G C, Kim M and Pennycook S J 2003 *Adv. Mater.* **15** 526
[6] Heo Y W, Kaufman M, Pruessner K, Norton D P, Ren F, Chisholm M F and Fleming P H 2003 *Solid-State Electron.* **47** 2269
[7] Morales A M and Leiber C M 1998 *Science* **279** 208
[8] Shi G, Mo C M, Cai W L and Zhang L D 2000 *Solid State Commun.* **115** 253
[9] Vayssieres L, Keis K, Hagfeldt A and Lindquist S 2001 *Chem. Mater.* **13** 4395
[10] Cao H, Zhao Y G, Ong H C, Ho S T, Dai J Y, Wu J Y and Chang R P H 1998 *Appl. Phys. Lett.* **73** 3656
[11] Hosono E, Fujihara S and Kimura T 2004 *Electrochem. Solid-State Lett.* **7** C49
[12] Agashe C, Kluth O, Hüpkes J, Zastrow U, Rech B and Wuttig M 2003 *J. Appl. Phys.* **95** 1911
[13] Li S Y, Lin P, Lee C Y and Tseng T Y 2004 *J. Appl. Phys.* **95** 3711
[14] Zhao D, Liu Y, Shen D, Lu Y, Zhang J and Fan X 2001 *J. Appl. Phys.* **90** 5561
[15] Shannon R D 1976 *Acta Crystallogr.* A **32** 145
[16] Makino T, Tuan N T, Sun H D, Chia C H, Segawa Y, Kawasaki M, Ohtomo A, Tamura K and Koinuma H 2000 *Appl. Phys. Lett.* **77** 975
[17] Du Y, Cai W L, Mo C M, Chen J, Zhang L D and Zhu X G 1999 *Appl. Phys. Lett.* **74** 2951
[18] Wang J, Du G, Zhang Y, Zhao B, Yang X and Liu D 2004 *J. Cryst. Growth* **263** 269
[19] Vanheuseden K, Warren W L, Seager C H, Tallant D R, Voigt J A and Gnade B E 1996 *J. Appl. Phys.* **79** 7983
[20] Jo S H, Banerjee D and Ren Z F 2004 *Appl. Phys. Lett.* **85** 1407